JTTEE5 15:83-91
DOI: 10.1361/105996306X92640
1059-9630/$19.00 © ASM International

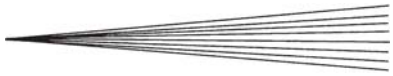

Ultrafast Thermal Plasma Physical Vapor Deposition of Yttria-Stabilized Zirconia for Novel Thermal Barrier Coatings

Heji Huang, Keisuke Eguchi, Makoto Kambara, and Toyonobu Yoshida

(Submitted July 28, 2005; in revised form October 20, 2005)

This research aims to develop advanced thermal plasma spraying technology for the next-generation thermal barrier coatings (TBCs) with a high power hybrid plasma spraying system. By using thermal plasma physical vapor deposition (TP-PVD), various functional structured yttria-stabilized zirconia (YSZ) coatings were deposited. Parameters, such as powder feeding rate, hydrogen gas concentration, and total mass flow rate of the plasma gas, were optimized, and their influences on the evaporation of YSZ powder were investigated. Ultrafast deposition of a thick coating was achieved at a rate of over 150 μm/min. The deposited porous coating has a low thermal conductivity of 0.7 W/mK and the dense coating with interlaced *t′* domains possesses a high nanohardness of 27.85 GPa and a high reflectance. These characteristics show that the TP-PVD technique is a very valuable process for manufacturing novel TBCs.

Keywords displacive transformation, hybrid plasma, thermal barrier coatings, thermal plasma (PVD), thermal plasma spraying

1. Introduction

With its unique physical and chemical properties (Ref 1), yttria-stabilized zirconia (YSZ) has been intensively studied and used in various applications, including solid oxide fuel cells (SOFCs), gas sensors, gas separation membranes, as a buffer layer for superconducting films, and, especially in recent years, in the application of thermal barrier coatings (TBC). The use of TBCs together with the development of superalloys and cooling systems enable the continuous improvements in the efficiency and durability of gas turbine engines. TBCs are not only applicable for modern superalloy engines but are also essential to protect ceramic matrix composite (CMC) components in the propulsion industry (Ref 2). Because the thickness of the TBCs must usually be over several hundreds of microns, deposition rate and cost efficiency have become the most important criteria for choosing the manufacturing methods. Generally, high-speed deposition processes such as atmospheric plasma spraying (APS) and electron-beam physical vapor deposition (EB-PVD) have been adopted for commercial applications. However, each of these methods has its own unique pros and cons, and these have been addressed in the literature; e.g., EB-PVD TBCs are strain tolerant with a good surface finish but possess relatively higher thermal conductivity and poorer affordability (due to high equipment costs, low material deposition efficiencies of 2-5% of the evaporated flux, and the relatively slow deposition rate of about 5 μm/min). Thus, to meet the requirements of the increased operation temperatures of next-generation TBCs, improvements of existing deposition techniques and developments of alternate routes to obtain high-quality YSZ coatings more effectively are indispensable.

Improvements of EB-PVD TBCs aim to reduce either the thermal conductivity or the processing costs. The former was mainly achieved by depressing the amount of the so-called type I intercolumn gaps with such morphologies as the "zig-zag" or the "herringbone" (Ref 3) and the multilayered top-coat by repeating the initial zone (Ref 4) or applying different kinds of doping. Improvements in the cost efficiency of the EB-PVD technique are due to advances in viable processing methods, e.g., the development of the EB-DVD (Ref 5), in which a carrier gas jet was introduced to rapidly create and efficiently transport evaporant to the substrate. On the other hand, the introduction of plasma has been found appealing to improve the vapor deposition rates of various materials, and this was interpreted as the result of accelerated transportation and deposition of coagulated clusters due to supersaturated vapor and thermophoretic effects within the boundary layer (Ref 6). Chae et al. (Ref 7) successfully deposited microcrystalline Si by thermal plasma chemical vapor deposition (TP-CVD) at a rate over 60 μm/min. Wang et al. (Ref 8, 9) also reported deposition of a SiC layer by thermal plasma physical vapor deposition (TP-PVD) at a rate of over 12 μm/min. For YSZ deposition, Goto et al. (Ref 10) reported a deposition rate of 11 μm/min by laser chemical vapor deposition (LCVD), where plasma was emerged near the substrate surface.

We propose herein a peculiar layered structure for TBCs and report the first results of a study to access the potential of YSZ TBCs synthesized by the TP-PVD method with a novel 300 kW twin hybrid plasma spraying (THPS) system. The advantages of the TP-PVD method are its simplicity, flexibility, together with minimum byproducts (Ref 11). In this process, powders are used as raw materials and injected into the plasma. The ability to cause vaporization is the most important feature. To expect perfect evaporation of the powders, small powders must be fed con-

Heji Huang, Keisuke Eguchi, Makoto Kambara, and **Toyonobu Yoshida,** Department of Materials Engineering, the University of Tokyo, Hongo, 7-3-1, Bunkyo-ku, Tokyo, Japan, 113-8656. Contact e-mail: huang@plasma.t.u-tokyo.ac.jp.

tinuously into the plasma. The development of a precisely controllable powder feeder enables this process to be applicable for various depositions.

2. TBC Structure Design

Figure 1 summarizes typical coating morphologies deposited by different growth mechanisms. If the coating is deposited directly from vapor to solid, a columnar structure is expected for most cases (Ref 12), which is typical of EB-PVD or jet-CVD processes (Fig. 1a); if a cluster forms in the boundary layer near the substrate during the vapor deposition, a nanoparticle structure is preferred, which is the case for TP-PVD and TP-CVD (Fig. 1b). If such vapor deposition is integrated with droplet deposition (e.g., thermal plasma powder spray, TP-PS), a peculiar layered structure composed both of powder sprayed "splats" and vapor-deposited nanoparticles or columns could be achieved, which is promising for colligating the merits of the present deposition techniques to maximize the properties of the TBC with minimum compromise (Fig. 1c); this was chosen as the ideal TBC structure in this research. In this design, the splats obtained by plasma powder spraying can act as radiation shields, and the columns or nanoparticles with nanocracks and pores help to reduce both photon and phonon transportation and to release the stress that accompanies drastic temperature changes. YSZ-based TBCs were significantly transparent to thermal radiation at wavelengths between 0.3 and 5 μm (Ref 13). Therefore, a quarter-wavelength filter for YSZ TBC (between λ/4 and λ) could be achieved if the layer periodicity is between 0.2 and 2 μm, which will increase the photon scattering significantly and weaken the radiation heating at high working temperatures over 1200 °C (Ref 14).

3. Experimental Procedures

A novel 300-kW twin hybrid plasma spraying system (Fig. 2) was developed in this study to deposit the desirable multilayered TBC. There are two key points in this design. First, two hybrid plasma torches (Ref 15) are positioned in the same chamber, each of which is capable of TP-PVD, TP-CVD, or TP-PS, if different source materials are fed into the torches. Second, a rotary substrate holder enables alternating exposure of the substrate to the two plasma flames, thus allowing cyclic deposition by TP-PVD, TP-CVD, or TP-PS, if different processes are assigned to the two hybrid plasma torches. A more detailed description of the specifications of the hybrid plasma torch is found elsewhere (Ref 16, 17). Figure 2 also shows various types of substrate holders used in this research to either study the effect of deposition distance with shelves of different heights (Fig. 2b) or to maintain the relative lower temperature of the stationary substrate during single-torch deposition by water cooling (Fig. 2c) or to eliminate the spatial variation of the coating thickness on the substrate by using a rotation/revolution type of holder (Fig. 2d). Hereafter, these are referred to as type I, II, III, and IV substrate holders for those showed in Fig. 2(a) to (d), respectively. The temperature on the backside of the substrate was measured with an R-type thermocouple for both rotary and stationary depositions. When water cooling was used, the temperatures at the inlet and the outlet of the holder were also monitored. The temperature data were collected directly into the computer by a data logger (Keyence NR500, Japan) with sample intervals of 100 ms.

Typical experimental parameters are listed in Table 1. To optimize the TP-PVD process, experiments were mainly conducted based on single-torch deposition. Six kinds of 8YSZ powders were used as feedstocks. By using a turntable-type powder feeder (Sulzer Metco Twin 10), the powder was fed into the torch at 0.3, 1, 2, 4, 6, and 9 g/min to investigate the effect of the powder feeding rate. A rather high chamber pressure of 300-500 torr was used in the current study. Compared with the conventional low-pressure PVD and CVD deposition of thin films, the influence of the substrate structure on the coating's microstructure was thought to be negligible in the TP-PVD process, because the vapor nucleates in the boundary layer instead of at the substrate surface, together with an order of magnitude difference on the thickness of the coating. Therefore, graphite was mainly used as substrate material in the current study instead of MCrAlY-coated metal to easily obtain the fractured cross section of the deposited coating for fine microstructure observation and to pre-

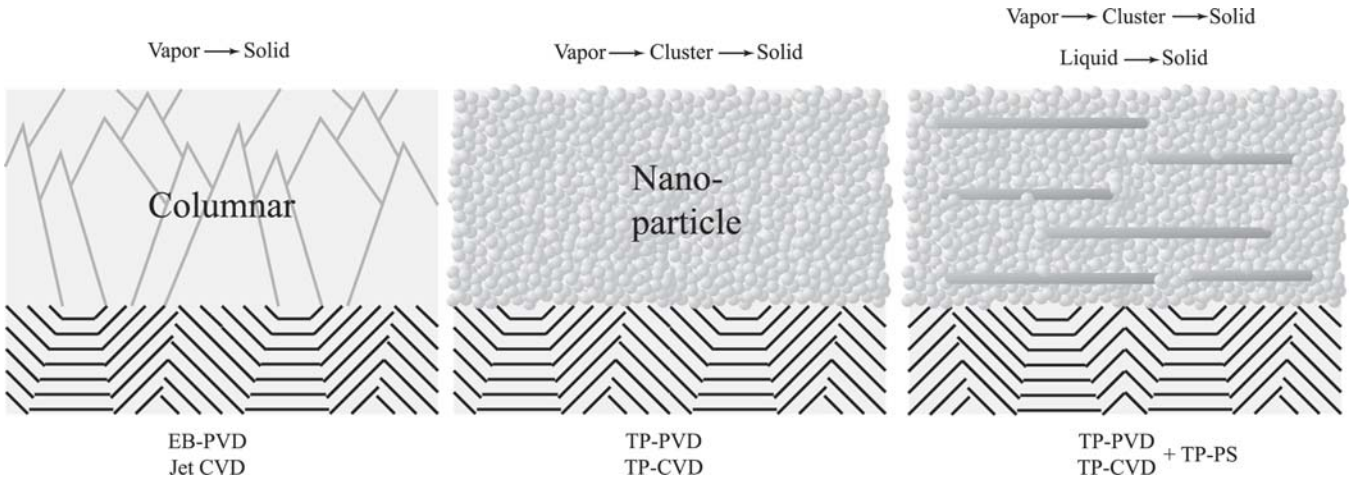

Fig. 1 Growth morphologies of coatings from different deposition mechanisms

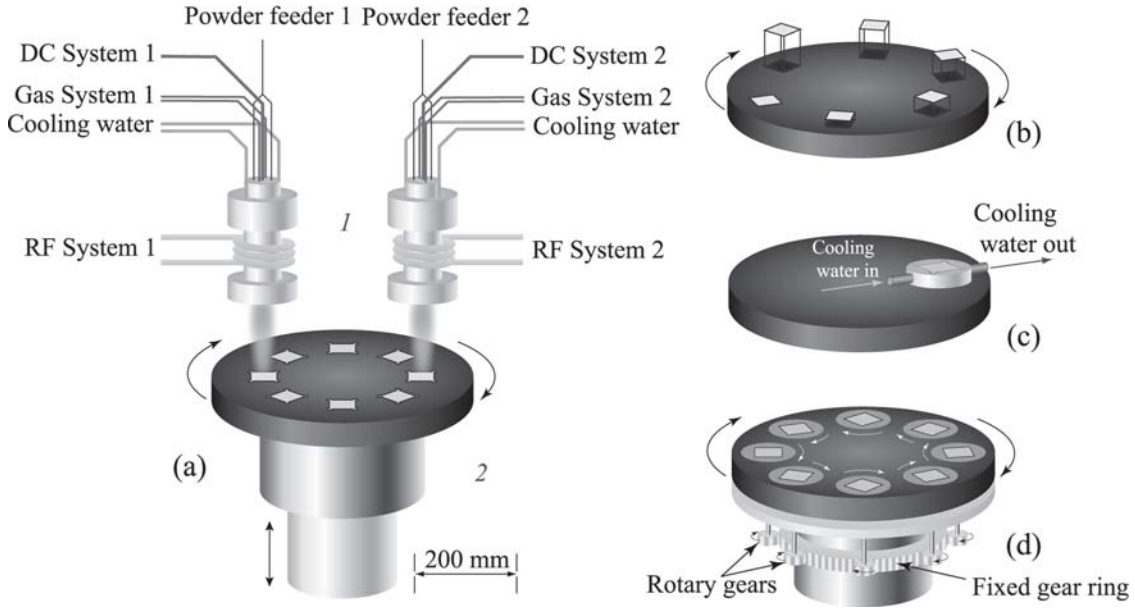

Fig. 2 Schematic diagram of the THPS system with different substrate holders: (a) original type; (b) shelves with different heights on the holder; (c) water-cooled stationary holder; and (d) planetary holder

Table 1 Typical experimental parameters

Parameters	Values
DC plasma, kW	7
DC plasma gas flow rate, slm	10
RF plasma power, kW	70, 100
RF plasma gas flow rate, slm	100, 200
Hydrogen concentration, vol%	10, 15, 20, 30
Powder feeding rate, g/min	0.3, 1, 2, 4, 6
Substrate material	CoNiCrAlY-coated alloy, Graphite
Substrate position, mm	30, 50, 70
Substrate rotation speed, rpm	0, 20, 50, 100
Substrate temperature, °C	500-1000
Chamber pressure, torr	300-500
Carrier gas flow rate, slm	4-6
Deposition time, min	3-15
Cooling water flow rate, L/min	26

pare a free-standing coating for thermal conductivity measurement. Ar/H_2 was used as the plasma gas because of its high thermal conductivity. Experiments to study the effect of hydrogen concentration (C_{H2}) were conducted at three different C_{H2} levels (10, 20, and 30 vol.%) with RF power of 100 kW, total gas flow rate of 200 slm, and powder feeding rate of 2 g/min. The effect of the flow rate of plasma gas was investigated with the total gas flow rates of 100 and 200 slm, respectively, (C_{H2} = 15 vol.%), while the powder feeding rate was kept at 2 g/min. The RF powers were 70 and 100 kW, respectively. The morphologies of the feedstock powders were observed by a laser microscope. The microstructures of the coatings were analyzed by field-emission scanning electron microscopy (FE-SEM), focused ion beam scanning electron microscopy (FIB-SEM), and high-resolution transmission electron microscopy (HRTEM). The phase was identified by x-ray diffractometry. A slow scan over 72-76° of 2θ with a 0.002° step was conducted to monitor the (400) cubic (*c*) and tetragonal (*t*) zirconia peaks. Peaks were analyzed by the Gaussian fit method.

4. Results and Discussion

4.1 Source Powder Selection

Powder used as feedstock for TP-PVD deposition should be properly small, narrowly distributed, and have a good ability to flow. Only if the size of the powder is small enough can effective heat transfer from the plasma be expected. Because the residence time of the powder in a hybrid plasma is usually on the order of milliseconds (Ref 11, 15), a powder that is too large cannot be fully evaporated and the liquid core will then remain and form a splat in the coating. On the other hand, if the powder is too small, it is difficult to maintain a steady feed, as small powders tend to form large agglomerates due to the large surface specific area and high surface energy. Furthermore, for a powder that is too small, because of its low inertia, it is difficult to gain enough momentum to penetrate into the plasma unless the carrier gas velocity is drastically increased. However, when the velocity of the carrier gas is too high, the plasma will be remarkably disturbed and become unstable (Ref 18), which will certainly reduce the coating quality. In the TP-PVD process, the narrow size distribution of the source powder should also be emphasized. This is because the size distribution significantly affects the velocity of the powder before it is injected into the plasma. Although a 20 μm difference between the largest and smallest powders has a trivial effect for large particles, this difference will significantly affect small ones and lead to totally different thermal histories of these particles.

Table 2 shows the laser micrograph of four kinds of the 8YSZ powders tested in TP-PVD feeding and deposition experiments. Two other powders (Sumitomo Cyclone and Sieved Amperit 825.0) have similar morphologies as the powders with the same manufacture; the only difference is in size. They are divided into two main types: the fused/crashed powder and the agglomerated powder. Agglomerated powders are characterized by a very

small crystal size (60 nm) and spherical agglomerated shapes. However, a large agglomerated powder (e.g., Tosoh TZ-3YS) cannot be fully evaporated and a small agglomerated powder (e.g., Sumitomo Cyclone) can easily block the feeding channel, especially near the DC torch exit. Fused and crushed 8YSZ powders of 5-15 μm (Amperit 825.090) are thought to be the best choice for TP-PVD in the present study, as it is small enough to be evaporated together with essential flowability for smooth feeding through the turntable-type powder feeder. Of course, it is much better if such particles are spherical. Unfortunately, a spherical powder with particle sizes of ~10 μm is not yet commercially available.

4.2 Optimization of Deposition Parameters

A previous study has shown that the powder feeding rate affects the evaporation condition of the fine powder significantly (Ref 17). Using the type I and II substrate holders, at 100-kW RF input power and 200 slm gas flow of 15 vol.% hydrogen concentration (C_{H2}), the microstructures of the deposited coatings varied from mostly sprayed splats to PVD nanostructures when the powder feeding rate was reduced from 4 to 1 g/min. At a powder feeding rate of 2 g/min, the peculiar layered coating consisting of both structures was deposited as designed. Figure 3(a) is the FIB-SEM cross-sectional view of the layered structure. Small splats with thickness around 500 nm are well dispersed in the matrix of the vapor-deposited columns. A relatively wide distribution of the thickness of the nanocolumns (h_v) of 0.1-1 μm was observed, which indicates an incomplete covering of the substrate surface. Due to the scanty powder feeding rate of 2 g/min, the paucity of splats cannot cover the whole surface of the substrate in one rotation through the plasma, while PVD structure continues to grow in each turn. Figure 3(b) shows a 3-dimensional diagrammatic sketch of a portion of this structure.

Feeding the source powder to the two torches with different rates of 9 and 2 g/min forms a very porous coating by using the

Table 2 Specifications of typical powders used in this research

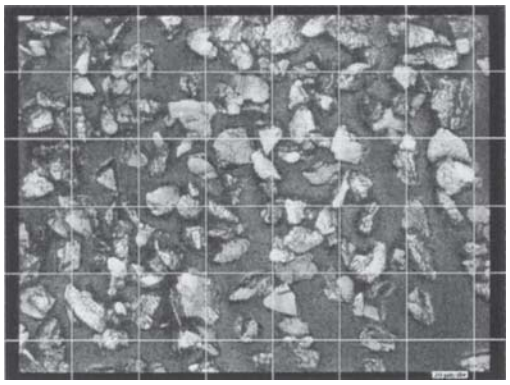

Company: H.C. Starck
Brand: Amperit 825.090
Fused 15/5 μm
Grain sizes measured:
- 22 μm, 100%
- 15 μm, 92%
- 10 μm, 64%
- 5.5 μm, 13%

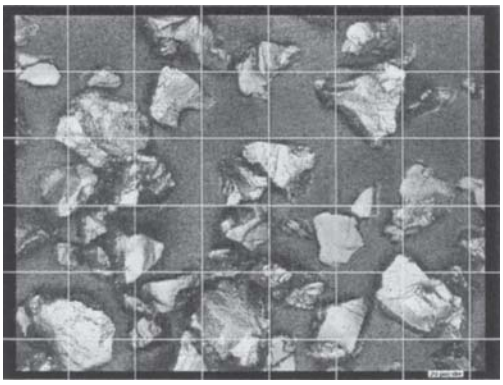

Company: H.C. Starck
Brand: Amperit 825.0
Fused 22.5-5.6 μm
Grain sizes measured:
- 62 μm, 100%
- 31 μm, 92%
- 5.5 μm, 2.1%

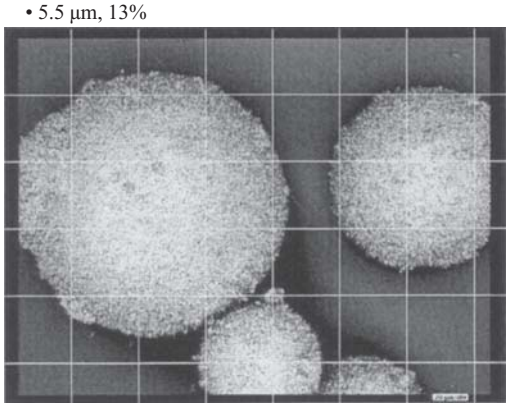

Company: Tosoh Corporation
Brand: TZ-3YS
Specific surface area: 13.0 m^2/g
Crystallite size: 250 Å

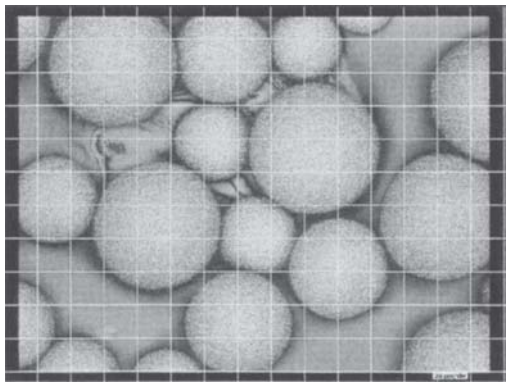

Company: Sumitomo Osaka Cement Co., Ltd.
Brand: OZC-3YFA
Specific surface area: 15.5 m^2/g
Crystallite size: 600 Å (average)
Size: 70-75 μm (average)

Scale: 20 μm/div

type I holder, as shown in Fig. 4. With the powder feeding rate as high as 9 g/min, the plasma was much cooled down, and the melted droplets resolidified before impinging onto the substrate, thus formed the spherical balls in the coating. The thickness of the coating is 650 μm and was deposited in only 10 min. The thermal diffusivity of a free-standing sample with the same structure was measured to be 5.31×10^{-6} m^2/s, and due to the

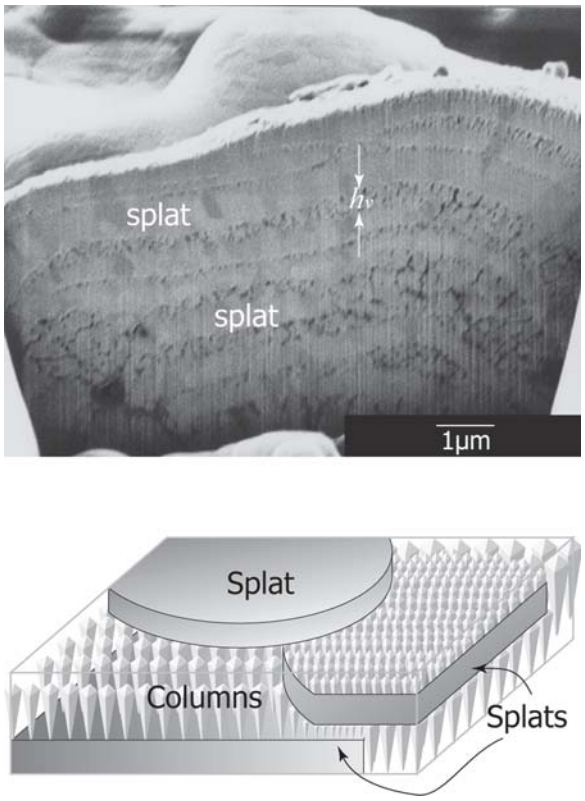

Fig. 3 Peculiar layered structure consisting both of powder sprayed splats and vapor deposited nano-columns: (a) FIB-SEM micrograph; (b) diagrammatic sketch

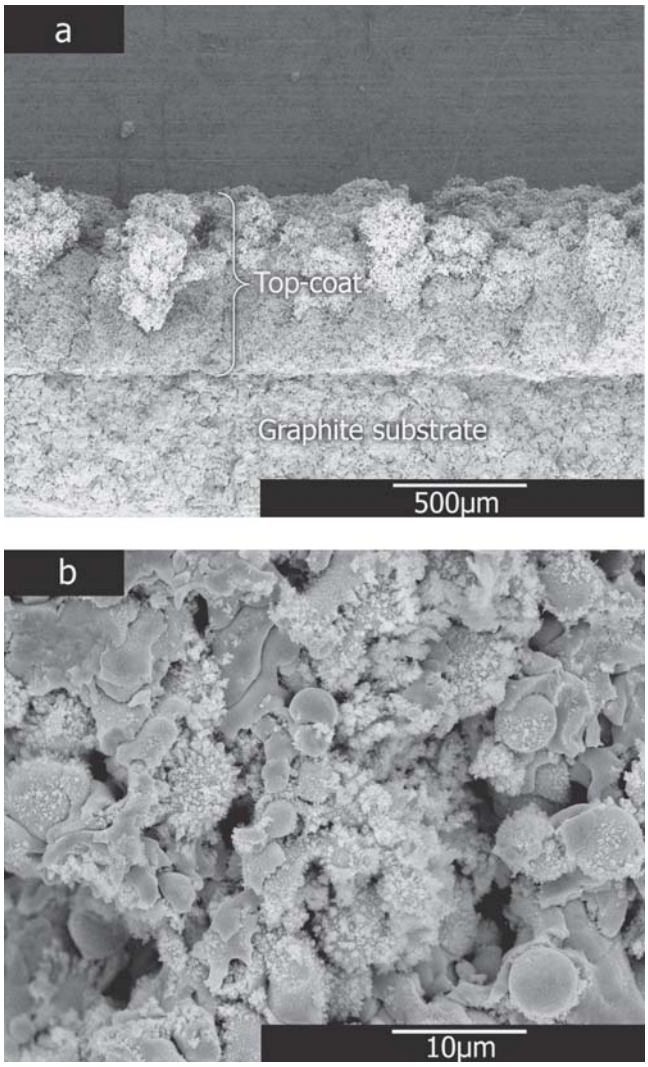

Fig. 4 FE-SEM micrographs of the porous coating prepared by twin-torch deposition with powder feeding rate of 9 and 2 g/min, respectively, at (a) low and (b) high magnification

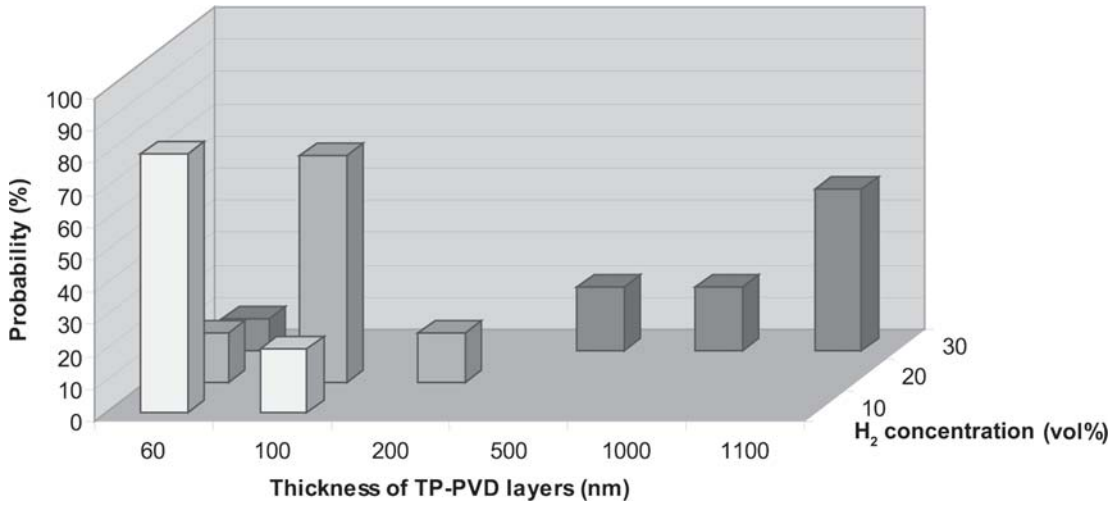

Fig. 5 Effect of hydrogen concentration on the thickness of the TP-PVD layer at powder feeding rate of 2 g/min

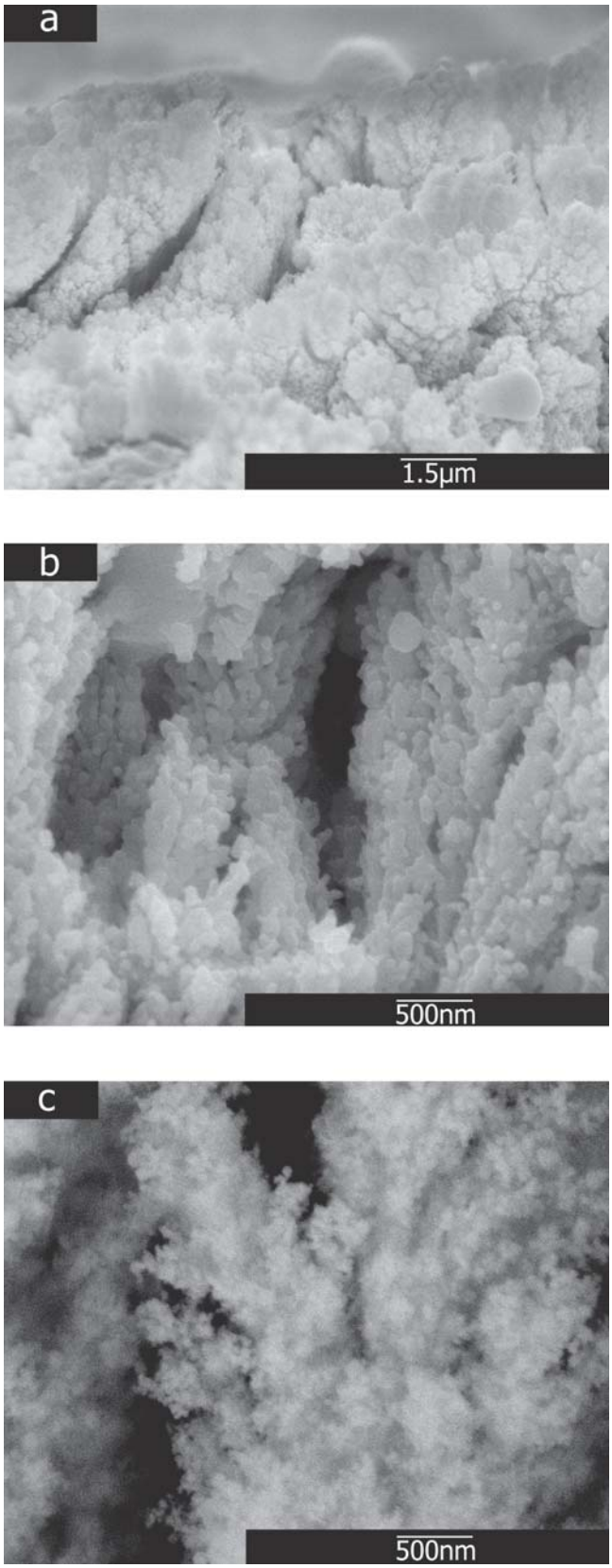

Fig. 6 Cross-sectional micrograph of TP-PVD coating deposited on rotary substrate with different chamber pressures: (a, b) 300 torr; (c) 500 torr

low density of 2.63 g/cm^3, the thermal conductivity is as low as 0.7 W/mK at room temperature.

Figure 5 shows the distribution of the thickness of the TP-PVD layer (h_v, as marked in Fig. 3a) at different C_{H2}, which reveals the dependence of the average vaporization condition on hydrogen concentrations. h_v increases with the increase of C_{H2}: when C_{H2} is only 10 vol.%, h_v centralizes around 60 nm; when C_{H2} is 30 vol.%, h_v increases to over 1 μm, which means much more powder has been evaporated. However, further increase of C_{H2} is unfavorable under present experimental conditions, as extra power is needed to maintain the stability of the plasma.

With the powder feeding rate of 2 g/min, complete evaporation was achieved by reducing the total flow rate of plasma gas from 200 to 100 slm. This is because the YSZ powder that had been injected into the plasma was accelerated mainly by the drag force, which is roughly proportional to the velocity of the plasma as the Reynolds number is in the order of 10-10^2. A longer residence time of the powder in the plasma is expected with a lower gas flow, which is beneficial for the evaporation of the powder. Figure 6 shows the fractured cross section of the YSZ coating deposited on the type II substrate at a substrate temperature of 800 °C, the deposited coating exhibits cauliflower structure, as shown in Fig. 6(a). In such rotary depositions, the substrate moved in and out of the plasma flame cyclically, which periodically interrupted the vapor flux and disturbed the continuous growth of the coating along preferred crystal direction. The size of the nanoparticles that build up the cauliflower structure changes with different chamber pressures. At a lower chamber pressure of 300 torr, the particle size is ~100 nm (Fig. 6b); when the chamber pressure was increased to 500 torr, the nanoparticles size is smaller, ~20-40 nm (Fig. 6c). This size change indicates that, at higher chamber pressure, collision occurs intensively and that most of the deposition comes from clusters. In the case of lower chamber pressures, however, some amount of the deposition still comes directly from the vapor due to the lower probability of collisions, which makes the nanoparticles grow more to a larger scale.

Figure 7(a) shows the fractured cross section of the TP-PVD coating deposited on the type III substrate. Two-step growth is clearly seen. The initial part consists of a fine columnar structure with a column width between 30 and 100 nm. When the columns grow, a faceted structure can be seen. The distance between the faceted steps is on the order of 100 nm. Convolution of such growth could be explained by the empirical structure zone model (Ref 12). In such a stationary substrate deposition, because the substrate is water-cooled, the initial layer grows at a lower temperature where there is insufficient surface diffusion of atoms and the shadowing effect dominates the formation of the columnar structure. When the thickness of the coating increases, due to the low thermal conductivity of zirconia, the followed coating is actually deposited on the previous layer with elevated temperature, thus leading to a faceted morphology. At even higher temperatures, for example, when the stationary substrate is not water-cooled, the columns become denser and competition growth can be observed (Fig. 7b).

Denser microstructure was observed in a much thicker TP-PVD YSZ coating deposited on a water-cooled stationary substrate. The dense coating, ~550 μm thick, was deposited in 3.5 min with an ultrahigh deposition rate over 150 μm/min. Figure 8(a) shows the fractured cross section of the coating. Fine nano-

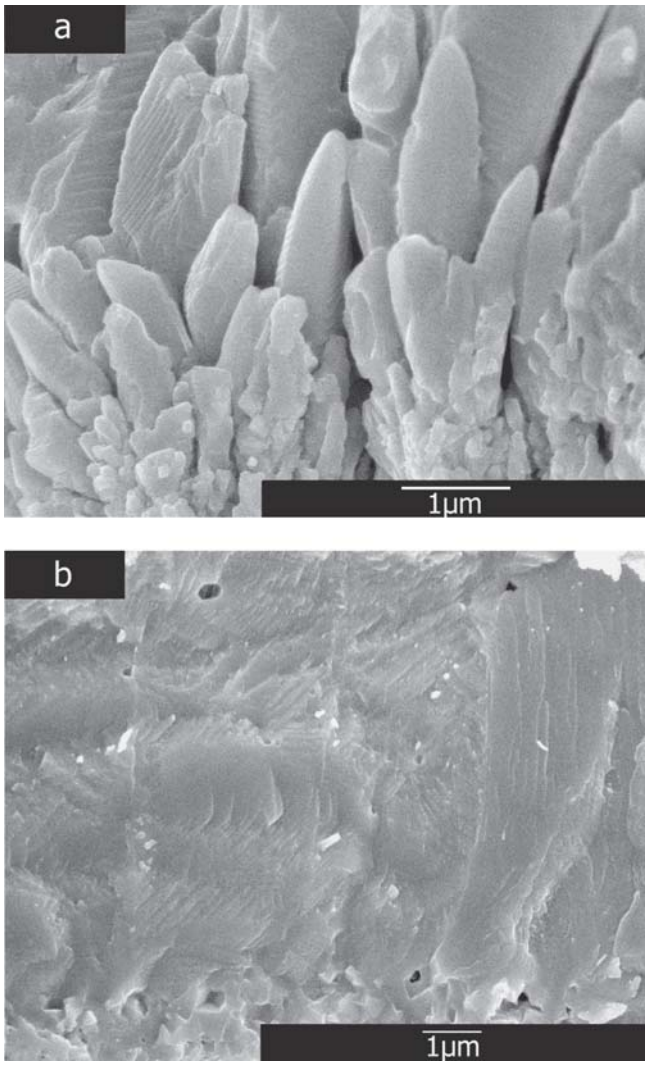

Fig. 7 FE-SEM micrographs of the cross section of TP-PVD YSZ coatings deposited on stationary substrate with (a) and without (b) water cooling.

faceted structure can be clearly seen in 50,000× FE-SEM micrographs, which show characteristic vapor deposition. The distance between two faceted steps is also ~100 nm, similar to that in Fig. 7(a). The polished cross section of the coating is very dense with few pores (Fig. 8b). However, after 5 min of etching 50% HF, interlaced structures appeared, as shown in Fig. 8(c). From TEM observations, such interlaced twin variants were seen more clearly (Fig. 9a), which suggests that the coating is mainly in t' phase. The size of the grains changes from ~5 μm to >10 μm from the bottom to the surface of the coating. The [001] diffraction pattern shows that there is no monoclinic phase. The (112)-type forbidden reflections are typically found in t-ZrO_2 but not in c-ZrO_2. HRTEM photo of the twin boundary is shown in Fig. 9(b) with incident beam in [110] direction. The lattice is continuous across the boundary and the interface plane is $[1\bar{1}0]$. EDS analysis for the three grains shows an average composition of about 5 mol% Y_2O_3. The t' phase can be formed at this composition of Y_2O_3 when the displacive c to t transformation oc-

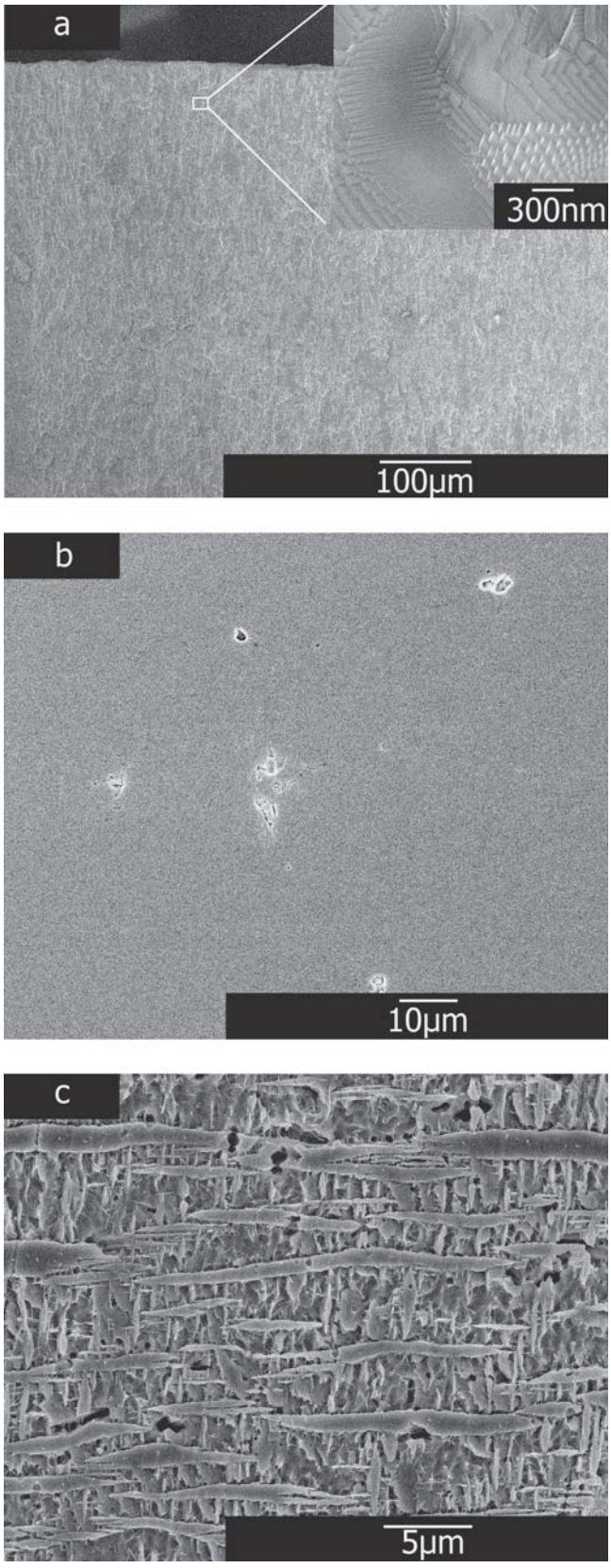

Fig. 8 Cross-sectional micrographs of dense YSZ coating deposited on water-cooled stationary substrate: (a) fracture morphology; (b) polished cross section; (c) etched morphology showing interlaced structure

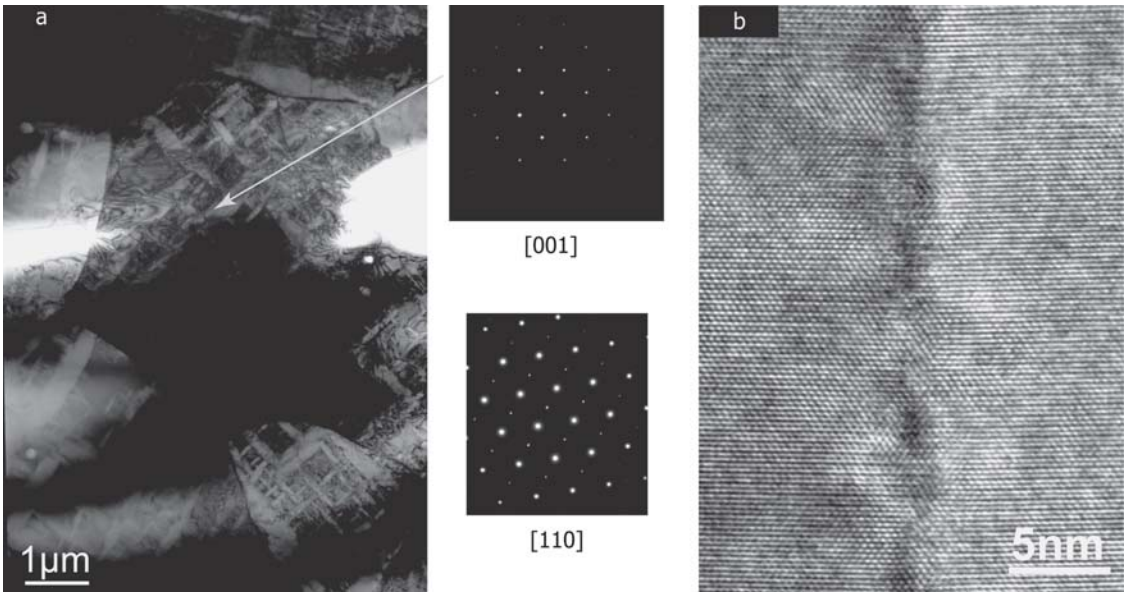

Fig. 9 TEM analysis of the interlaced structure: (a) dark-field image; (b) HRTEM micrograph of the boundary of the twin variants. The incident beam is in the [110] direction.

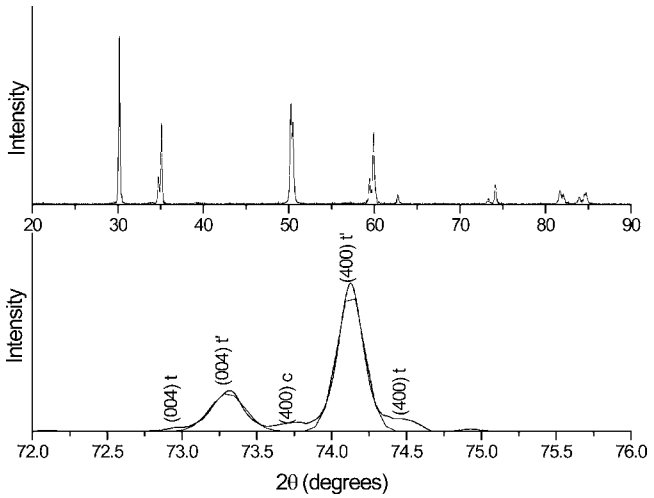

Fig. 10 XRD patterns of the coating

curs (Ref 19, 20). XRD patterns (Fig. 10) confirm that there is no *m*-ZrO_2. The slow scan over the (400) region between 72 and 76° (Fig. 10b) shows that the main peaks come from *t*′ phase, whereas very small amounts of *t* and c phase exist. The phase composition indicates that no martensitic transformation occurs in the coating. With such a dense and interlaced structure, the coating is very hard with nano- and microhardnesses of 27.85 and 12.32 GPa, respectively (Ref 21). Although the thermal conductivity of such coating is a bit higher (1.9 W/mK) (Ref 22), it is feasible in applications as an outer layer for a TBC system for improving the resistance of foreign object impact. Furthermore, the reflectance of this structure is much higher than that of the conventional APS and EB-PVD coatings, which adds the advantage in suppressing radiative heating, particularly at high temperatures (Ref 22).

5. Conclusions

The TP-PVD technique has been demonstrated to be a suitable approach to deposit YSZ coatings with a fine YSZ powder as the feedstock. The effects of powder feeding rate, hydrogen gas concentration, and total mass flow rate of the plasma gas on the evaporation of YSZ powder were investigated. Compared with the conventional EB-PVD process, the advantages of the TP-PVD method are ultrafast deposition rate (as high as 150 μm/min) and the flexibility. A thick coating over 500 μm can be deposited in only 3 min. Columnar structures similar to those deposited by EB-PVD as well as peculiar microstructures can be deposited by changing deposition parameters. A YSZ coating with thermal conductivity as low as 0.7 W/mK has been manufactured. Interlaced *t*′-ZrO_2 twins were found inside a dense YSZ coating, which had not been reported previously from vapor depositions, and these are thought to correspond to improved hardness and thermal reflectance.

Acknowledgments

The authors express their thanks to Dr. Shibata of the University of Tokyo for his skillful operation of the HRTEM. The present research is promoted by the NEDO nano-coating project.

References

1. X. Cao, R. Vassen, and D. Stoever, Ceramic Materials for Thermal Barrier Coatings, *J. Eur. Ceram. Soc.,* 2004, 24 (1), p 1-10
2. I. Spitsberg and J. Steibel, Thermal and Environmental Barrier Coatings for SiC/Sic CMCs in Aircraft Engine Applications, *Int. J. Appl. Ceram. Technol.,* 2004, 1 (4), p 291-301
3. S. Gu, T. Lu, D. Hass, and H. Wadley, Thermal Conductivity of Zirconia Coatings with Zig-Zag Pore Microstructures, *Acta Mater.,* 2001, 49 (13), p 2539-2547

4. J. Singh, D. Wolfe, R. Miller, J. Eldridge, and D. Zhu, Tailored Microstructure of Zirconia- and Hafnia-Based Thermal Barrier Coatings with Low Thermal Conductivity and High Hemispherical Reflectance by EB-PVD, *J. Mater. Sci.,* 2004, 39 (6), p 1975-1985
5. D. Hass, P. Parrish, and H. Wadey, Electron Beam Directed Vapor Deposition of Thermal Barrier Coatings, *J. Vac. Sci. Technol. A,* 1998, 16 (6), p 3396-3401
6. P. Han and T. Yoshida, Numerical Investigation of Thermophoretic Effects on Cluster Transport During Thermal Plasma Deposition Process, *J. Appl. Phys.,* 2002, 91 (4), p 1814-1818
7. Y. Chae, H. Ohno, K. Eguchi, and T. Yoshida, Ultrafast Deposition of Microcrystalline Si by Thermal Plasma Chemical Vapor Deposition, *J. Appl. Phys.,* 2001, 89 (12), p 8311-8315
8. X. Wang, K. Eguchi, C. Iwamoto, and T. Yoshida, Ultrafast Thermal Plasma Physical Vapor Deposition of Thick SiC Films, *Sci. Technol. Adv. Mater.,* 2003, 4 (2), p 159-165
9. X. Wang, K. Eguchi, C. Iwamoto, and T. Yoshida, High-Rate Deposition of Nanostructured SiC Films by Thermal Plasma PVD, *Sci. Technol. Adv. Mater.,* 2002, 3 (4), p 313-317
10. T. Goto, High-Speed Deposition of Zirconia Films by Laser-Induced Plasma CVD, *Solid State Ionics,* 2004, 172 (1-4), p 225-229
11. T. Yoshida, The Future of Thermal Plasma Processing for Coating, *Pure Appl. Chem.,* 1994, 66 (6), p 1223-1230
12. J. Thornton, High-Rate Thick-Film Growth, *Annu. Rev. Mater. Sci.,* 1977, 7, p 239-260
13. J. Nicholls, K. Lawson, D. Rickerby, and P. Morrel, Advanced Processing of TBC's Reduced Thermal Conductivity, *NATO Workshop on Thermal Barrier Coatings,* Aalborg, Denmark, 1998
14. R. Peterson, Direct Simulation of Phonon-Mediated Heat-Transfer in a Debye Crystal, *J. Heat Transfer Trans ASME,* 1994, 116 (4), p 815-822
15. T. Yoshida, T. Tani, H. Nishimura, and K. Akashi, Characterization of a Hybrid Plasma and Its Application to a Chemical Synthesis, *J. Appl. Phys.,* 1983, 54 (2), p 640-646
16. H. Huang, K. Eguchi, and T. Yoshida, High-Power Hybrid Plasma Spraying of Large Yttria-Stabilized Zirconia Powder, *J. Therm. Spray Technol.,* 2006, 15 (1), p 72-82
17. H. Huang, K. Eguchi, and T. Yoshida, Novel Structured Yttria-Stabilized Zirconia Coatings Fabricated by Hybrid Thermal Plasma Spraying, *Sci. Technol. Adv. Mater.,* 2003, 4, p 617-622
18. P. Fauchais, Understanding Plasma Spraying, *J. Phys. D: Appl. Phys.,* 2004, 37 (9), p R86-R108
19. A. Heuer, R. Chaim, and V. Lanteri, The Displacive Cubic-Tetragonal Transformation in ZrO_2 Alloys, *Acta Metall. Mater.,* 1987, 35 (3), p 661-666
20. R. Chaim, M. Ruhle, and A. Heuer, Microstructural Evolution in a ZrO_2-12 Wt-Percent Y_2O_3 Ceramic, *J. Am. Ceram. Soc.,* 1985, 68 (8), p 427-431
21. J. Li, H. Huang, K. Eguchi, M. Kambara, and T. Yoshida, Microstructural Investigation of YSZ Thermal Barrier Coatings Fabricated by Hybrid Plasma Spraying, *17th International Symposium on Plasma Chemistry*, August 7-12, 2005, p 969-970
22. T. Ma, M. Kambara, H. Huang, and T. Yoshida, Effect of Microstructure on Reflectance of Thermal Barrier Coatings, submitted